This appendix is in connection with Section 3.4.2 in the main report – Reaeration. Reaeration is an important contributor to DO gain in the tidal river. Novel formulations to improve representation of reaeration in WASP are introduced in this study. This appendix outlines: (1) an improved method of representing surface DO concentration in reaeration formulation; and (2) a reaeration formula which takes advantage of the turbulence closure formulation in EFDC. Benefits of our improved formulations are demonstrated.

1. IMPACT OF VERTICAL SEGMENTATION ON AMMONIUM AND OXYGEN PROFILES IN ESTUARIES

By Steven C. Chapra

INTRODUCTION

There are two key issues related to the correct representation of oxygen gas transfer for the Delaware Estuary Oxygen/Eutrophication Model:

1. Calculation of the impact of wind and water velocity on the liquid-film mass transfer coefficient.
2. Proper representation of gas transfer across the air-water interface.

The current note deals with the second issue. The first will be addressed elsewhere.

MODEL DEVELOPMENT

The estuary water column is idealized as a one-dimensional system with vertical transport via turbulent diffusion and longitudinal transport neglected. Mass balances for ammonium and dissolved oxygen can be written as:

$$\frac{\partial n_a}{\partial t} = \frac{\partial}{\partial z}\left(E\frac{\partial n_a}{\partial z}\right) - \frac{o}{K_{so}+o}k_{nitr}n_a \tag{1.1}$$

$$\frac{\partial o}{\partial z} = \frac{\partial}{\partial z}\left(E\frac{\partial O}{\partial z}\right) - r_{on}\frac{o}{K_{so}+o}k_{nitr}n_a \tag{1.2}$$

where E = vertical eddy diffusivity (m^2/d); z = depth (m); n_a = ammonium (mgN/L); o = dissolved oxygen (mgO_2/L); K_{so} = half-saturation constant for low oxygen attenuation of nitrification (mgO_2/L); k_{nitr} = nitrification rate (/d); and r_{on} = ratio of oxygen consumed to ammonia nitrified = 4.57 mgO_2/mgN. Depth increases downward from the air-water interface, defined as $z = 0$.

A constant flux of ammonium, J_N ($gN/(m^2 \cdot d)$), is fed into the system at the sediment-water interface. A temperature-dependent constant sediment oxygen demand, *SOD* ($gO_2/(m2 \cdot d)$), removes oxygen at the sediment-water interface. A flux of oxygen, J_O ($gO^2/(m^2 \cdot d)$), enters the system across the air-water interface as a function of the difference between the oxygen saturation, o_s (mgO_2/L) and the air-water interface oxygen concentration, $o(0)$:

$$J_O = K_L\left(o_s - o(0)\right) \tag{1.3}$$

where K_L = the mass-transfer coefficient of oxygen (m/d).

As depicted in Figure 1-1, a numerical solution of Eqs. (1.1) and (1.2) can be developed by dividing the water column into a series of control volumes of equal thickness, Δz (m). This converts the partial differential equations into a system of ordinary differential equations (the so-called "Method of Lines"). Mass balances can be written for ammonia and oxygen for each of the interior volumes (i = 2 to n – 1) as:

$$\frac{dn_{a,i}}{dt} = \frac{E}{\Delta z^2}\left(n_{a,i-1} - n_{a,i}\right) + \frac{E}{\Delta z^2}\left(n_{a,i+1} - n_{a,i}\right) - \frac{o_i}{K_{so}+o_i}k_{nitr}\,n_{a,i} \tag{1.4}$$

$$\frac{do_i}{dt} = \frac{E}{\Delta z^2}\left(o_{i-1} - o_i\right) + \frac{E}{\Delta z^2}\left(o_{i+1} - o_i\right) - r_{on}\frac{o_i}{K_{so} + o_i}k_{nitr}\, n_{a,i} \tag{1.5}$$

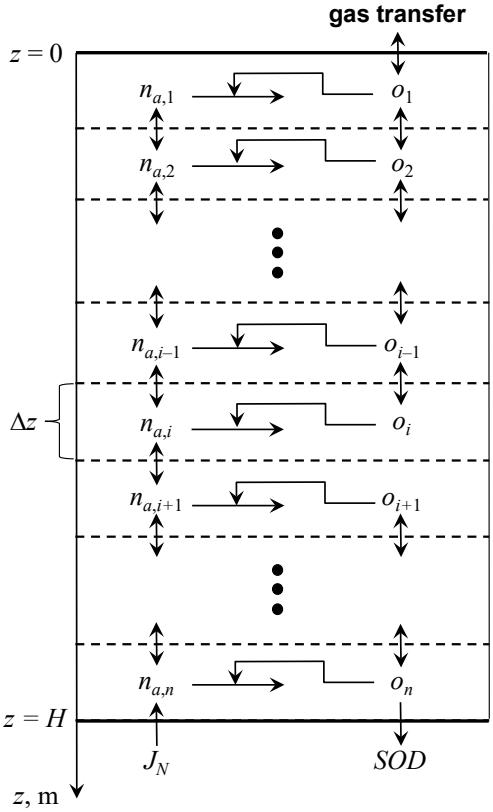

Figure 1-1: Control-volume segmentation of the water column for ammonium and dissolved oxygen.

For the bottom control volume ($i = n$), the equations must include the sediment-water fluxes as well as reflect that there is no additional transport across the sediment-water interface:

$$\frac{dn_{a,n}}{dt} = \frac{E}{\Delta z}\left(n_{a,n-1} - n_{a,n}\right) - \frac{o_n}{K_{so} + o_n}k_{nitr}\, n_{a,n} + \frac{J_N}{\Delta z} \tag{1.6}$$

$$\frac{do_n}{dt} = \frac{E}{\Delta z}\left(o_{n-1} - o_n\right) - r_{on}\frac{o_n}{K_{so} + o_n}k_{nitr}\, n_{a,n} - \frac{SOD}{\Delta z} \tag{1.7}$$

For the top control volume ($i = 1$), the ammonium balance is straightforward in that the only modification is that there is no diffusion between the air and the water:

$$\frac{dn_{a,1}}{dt} = \frac{E}{\Delta z^2}\left(n_{a,2} - n_{a,1}\right) - \frac{o_1}{K_{so} + o_1}k_{nitr}\, n_{a,1} \tag{1.8}$$

For the oxygen balance, gas transfer across the air-water interface must be included. This is typically done in water-quality models by assuming that the oxygen concentration of the first control volume is an adequate approximation of the concentration at the air-water interface; i.e., $o(0) \cong o_1$. With this assumption, the oxygen mass balance for the top control volume is written as:

$$\frac{do_1}{dt} = \frac{E}{\Delta z}(o_2 - o_1) - r_{on}\frac{o_1}{K_{so} + o_1}k_{nitr}\, n_{a,1} + \frac{K_L}{\Delta z}(o_s - o_1) \tag{1.9}$$

MODEL APPLICATIONS

Example simulations were implemented for a 10-m water column with the following parameters: E = 8.64 m^2/d (1 cm^2/s), r_{on} = 4.57 mgO_2/mgN, k_{nitr} = 0.1/d, K_{so} = 0.6 mgO_2/L, K_L = 1 m/d, o_s = 10 mgO_2/L, J_N = 1000 mgN/(m^2·d), and SOD = 0.5 gO_2/(m^2·d). Several cases representing different numbers of control volumes were employed: n = 4, 8, 12, and 16, which correspond to Δz = 2.5, 1.25, 0.8333, and 0.625 m, respectively.

In each case, the model was run to steady state to produce vertical profiles. As depicted in Figure 1-2, whereas the results for ammonium are relatively consistent, the oxygen profiles are highly sensitive to the number of volumes (or, alternatively, the volume thicknesses). First, notice that the oxygen profiles are very similar in shape regardless of the number of volumes. This connotes that, as would be expected for pure diffusive transport represented by centered differences, numerical diffusion (2nd-order) is negligible. However, the profiles are progressively offset to the right as the segmentation becomes cruder (i.e., fewer, thicker volumes). As described next, this is a direct result of the inadequacy of the assumption that the first control volume is an acceptable approximation of the concentration at the air-water interface in Eq. (1.9).

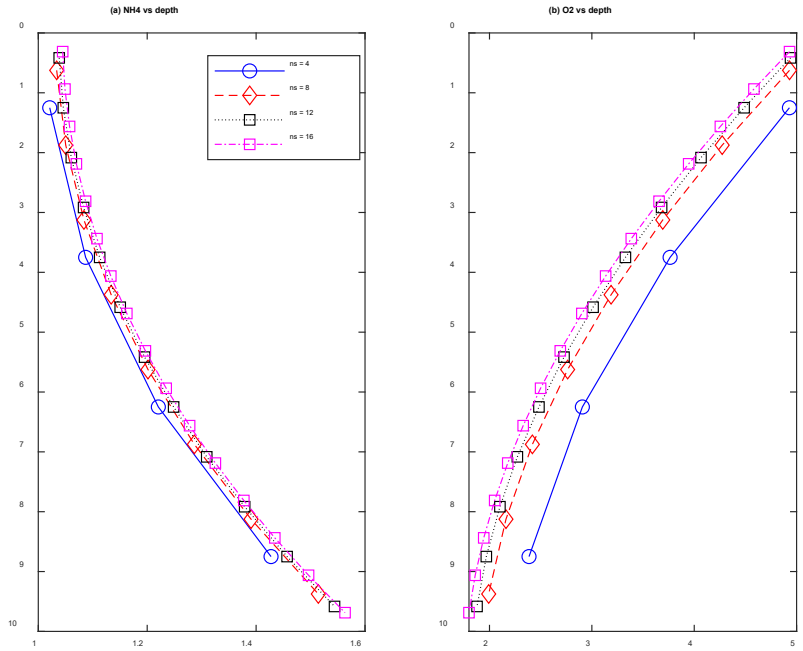

Figure 1-2: Profiles of (a) ammonia and (b) dissolved oxygen as computed with a numerical model for several cases with different number of layers and control-volume

thicknesses. For this case, it is assumed that the first control volume is an adequate approximation of the concentration at the air-water interface.

The previous example exhibits a fatal flaw; that is, gas transfer depends on the control-volume thicknesses. This deficiency can be rectified by more accurately estimating $o(0)$. Rather than assuming that the concentration of the first volume is an adequate approximation of the air-water interface concentration, a more physically realistic approach would be to extrapolate the trend with depth exhibited by several control volume concentrations.

As depicted in Figure 1-3, linear interpolation can be used to generate a straight line between the concentrations of the first two control volumes, which can then be extrapolated to estimate the concentration at the air-water interface. For our equal thickness grid, the linear interpolation formula is simply:

$$\boldsymbol{o(0) = o_1 - \frac{o_2 - o_1}{2} = 1.5o_1 - 0.5o_2} \tag{1.10}$$

As can be seen by summing the coefficients, the extrapolation consists of a weighted average of the two concentrations. For example, if $o_1 = 4$ and $o_2 = 2$:

$$o(0) = 1.5(4) - 0.5(2) = 5 \tag{1.11}$$

This refinement can be incorporated into the model by rewriting Eq. (1.9) as:

$$\frac{do_1}{dt} = \frac{E}{\Delta z}(o_2 - o_1) - r_{on}\frac{o_1}{K_{so} + o_1}k_{nitr}\, n_{a,1} + \frac{K_L}{\Delta z}(o_s - 1.5o_1 + 0.5o_2) \tag{1.12}$$

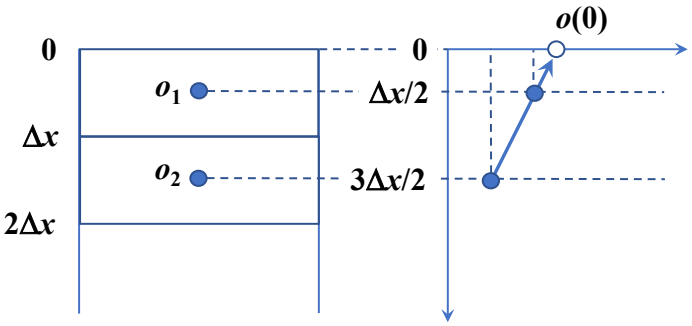

Figure 1-3: Estimation of the interface oxygen concentration via linear extrapolation of the concentrations of the first two control volumes.

With this modification, the example simulation results in Figure 1-4 are far superior to those when the first volume concentration was used to represent the interface concentration (Figure 1-2). For dissolved oxygen, the solutions for all four segmentations are consistent; even the crudest four-volume version ($n = 4$) is very similar to the more refined segmentations. As an ancillary benefit, because oxygen and nitrogen are coupled, the ammonium profiles are also improved, with all levels of resolution almost coincident.

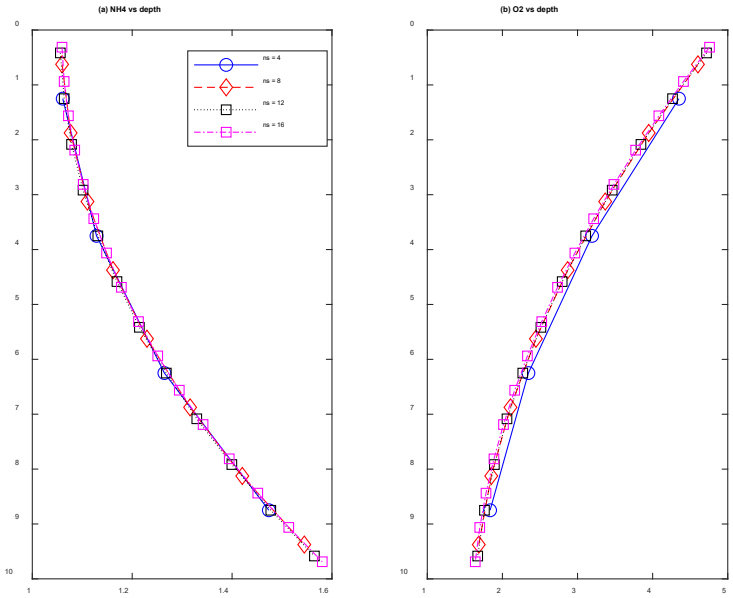

Figure 1-4: Profiles of (a) ammonia and (b) dissolved oxygen as computed with a numerical model for several cases with different number of layers and control-volume thicknesses. For this case, extrapolation of the linear near-surface trend is used to obtain a superior estimate of the concentration at the air-water interface.

To capture any curvature in the profiles, we can take this approach one step farther by fitting a second-order polynomial through the top three segments (Figure 1-5). A Lagrange second-order polynomial can be written as (Chapra 2018),

$$f(x)=\frac{(x-x_2)(x-x_3)}{(x_1-x_2)(x_1-x_3)}f(x_1)+\frac{(x-x_1)(x-x_3)}{(x_2-x_1)(x_2-x_3)}f(x_2)+\frac{(x-x_1)(x-x_2)}{(x_3-x_1)(x_3-x_2)}f(x_3) \qquad (1.13)$$

where f(x) is the dependent variable at the desired value of the independent variable x, and the subscript i designates the center of the ith volume. Note that this version could be employed for cases with unequally-spaced grids.

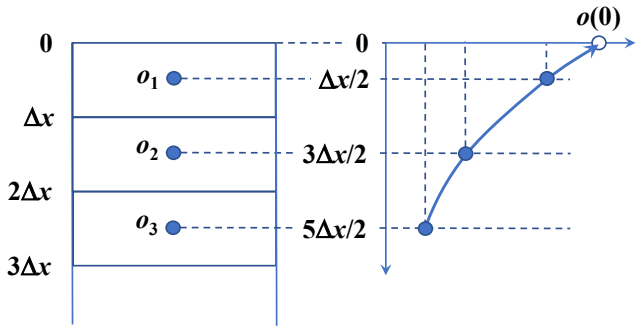

Figure 1-5: Estimation of the interface oxygen concentration via extrapolation of a quadratic interpolating polynomial based on the concentrations of the first three control volumes.

For our problem context, we can capitalize on the equal-spaced grid to develop a simplified application. We are interested in determining the oxygen concentration at the air-water interface, $o(0)$, given:

$$x_1 = 0.5\Delta z \qquad f(x_1) = o_1$$

$$x_2 = 1.5\Delta z \qquad f(x_2) = o_2$$

$$x_3 = 2.5\Delta z \qquad f(x_3) = o_3$$

Therefore, Eq. (1.13) can be written as:

$$o(0) = \frac{(0-1.5h)(0-2.5h)}{(0.5h-1.5h)(0.5h-2.5h)}o_1 + \frac{(0-0.5h)(0-2.5h)}{(1.5h-0.5h)(1.5h-2.5h)}o_2 + \frac{(0-0.5h)(0-1.5h)}{(2.5h-0.5h)(2.5h-1.5h)}o_3 \qquad (1.14)$$

where $h = \Delta z$. Collecting and cancelling terms yields:

$$o(0) = 1.875o_1 - 1.25o_2 + 0.375o_3 \qquad (1.15)$$

As with the linear version, the result again reduces to a simple weighted average. For example, if $o_1 = 4$, $o_2 = 2$, and $o_3 = 1$:

$$o(0) = 1.875(4) - 1.25(2) + 0.375(1) = 5.375 \qquad (1.16)$$

This refinement can be incorporated into the model by rewriting Eq. (1.9) as:

$$\frac{do_1}{dt} = \frac{E}{\Delta z}(o_2 - o_1) - r_{on}\frac{o_1}{K_{so} + o_1}k_{nitr}\, n_{a,1} + \frac{K_L}{\Delta z}(o_s - 1.875o_1 + 1.25o_2 - 0.375o_3) \qquad (1.17)$$

With this modification, results from the example simulation, shown in Figure 1-6, are superior to the previous versions. For dissolved oxygen, the solutions for all four segmentations are consistent, including the crudest four-volume version ($n = 4$).

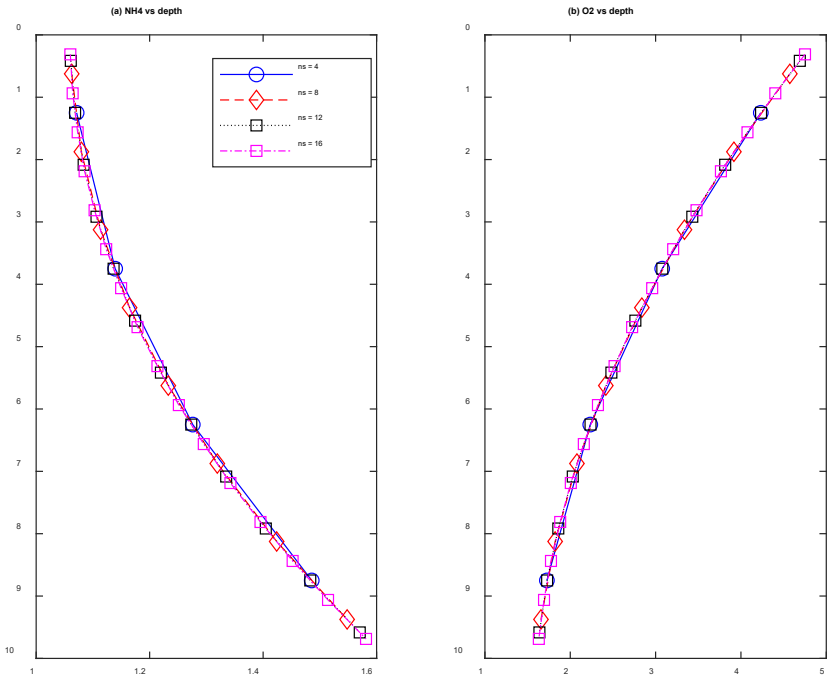

Figure 1-6: Estimation of the air-water interface oxygen concentration via extrapolation of a quadratic interpolating polynomial based on the concentrations of the first three control volumes.

OTHER CONSIDERATIONS

Shallow areas

Shallow parts of the system might consist of a single control volume (n = 1). For such zero-order cases, the interface concentration can be set equal to the volume's oxygen concentration:

$$o(0) = o_1 \tag{1.18}$$

Systems with unequal thicknesses

Some grids employ different volume thicknesses. In these cases, the general form of the Lagrange interpolating polynomial consists of a linear combination of Lagrange basis polynomials:

$$f_{n-1}(x) = \sum_{i=1}^{n} L_i(x) \cdot f(x_i) \tag{1.19}$$

$$L_i(x) = \prod_{\substack{j=1 \\ j \neq i}}^{n} \frac{x - x_j}{x_i - x_j} \tag{1.20}$$

where n = the number of data points, n – 1 = the order of the interpolating polynomial, and Π = the product operator. Inspection of these two equations makes it obvious that they yield the

interpolation/extrapolation equations employed above. For example, Eq. (1.13) corresponds to Eq. (1.19) and (1.20) with $n = 3$.

For the present problem context of estimating the oxygen at the air-water interface ($z = 0$), it can be rewritten using our nomenclature as:

$$o(0) = \sum_{i=1}^{n} L_i(0) \cdot o(z_i) \tag{1.21}$$

$$L_i(0) = \prod_{\substack{j=1 \\ j \neq i}}^{n} \frac{-o_j}{o_i - o_j} \tag{1.22}$$

A function to implement Eq. (1.21) can be developed in pseudocode as:

```
FUNCTION Lagrange(x, y, order)
n = order + 1
sum = 0
DOFOR i = 1, n
  product = yi
  DOFOR j = 1, n
    IF i ≠ j THEN
      product = product*(-xj)/(xi – xj)
    ENDIF
  END DO
  sum = sum + product
END DO
Lagrange = sum
END Lagrange
```

or in Fortran 95 as:

```
REAL FUNCTION lagrange(x, y, order)

! input:
!   x = vector of independent variables (depth)
!   y = vector of dependent variables (oxygen concentration)
!   order = order of polynomial (linear = 1, quadratic = 2)
! output:
!   lagrange = dependent variable at x = 0 (interface oxygen)

IMPLICIT NONE

INTEGER :: i, j
REAL(8) :: sum, product

n = order + 1
sum = 0
DO i = 1, n
  product = y(i)
  DO j = 1, n
    IF (i /= j) THEN
      product = product * (x(0) – x(j)) / (x(i) – x(j))
    END IF
  END DO
  sum = sum + product
END DO
Lagrange = sum
```

```
END FUNCTION lagrange
```

2. CALCULATE MASS TRANSFER COEFFICIENT WITH TURBULENCE DISSIPATION RATE

By Li Zheng, Ph.D.

Mass transfer coefficient and turbulence dissipation rate

Through field investigations in a wide range of aquatic and marine environments, Zappa et al. (2007) proposed quantifying air-water gas transfer based on the turbulent dissipation rate in the near-surface boundary layer:

$$K_L = \alpha(\varepsilon\nu)^{1/4}\, Sc^{-n} \tag{2.1}$$

where K_L = mass transfer coefficient at the air−water interface (m/s); α = proportional constant = 0.419 ± 0.130; ε = turbulent kinetic energy (TKE) dissipation rate (W/kg = m^2/s^3); ν = kinematic viscosity of water (m^2/s); *Sc* = Schmidt number for dissolved oxygen (DO), representing the ratio of momentum diffusivity (kinematic viscosity) and mass diffusivity; *n* = Schmidt number exponent, ranging from 1/2 to 2/3 depending on the surface conditions.

Zappa et al. (2007) notes that the gas transfer rate has different driving mechanisms that depend on wind conditions. These mechanisms include near-surface turbulence caused by low to moderate wind speeds (e.g., <10 m/s), and bubble-mediated exchange that likely becomes a significant factor when breaking waves are generated under higher wind speed conditions. Equation (2.1) is applicable only to the first condition, i.e., low to moderate wind speeds (Zappa et al., 2007). Research studies suggest that the turbulence dissipation rate, ε, ranges from 10^{-6} to 10^{-4} W/kg in energetic mixed layers when breaking waves are not occurring (Zappa et al., 2007) and 10^{-5} to 10^{-2} W/kg during conditions where breaking waves are occurring (Agrawal et al., 1992 and Terray et al., 1996).

In this study, the turbulence dissipation rate ε was estimated from the hydrodynamic model EFDC and transferred to the water quality model WASP through linkage files; ν and *Sc* were calculated in WASP; and an upper-bound of 10^{-4} W/kg was set for ε to ensure Eq. (2.1) was applied properly and sporadic large ε values, likely representative of breaking wave conditions, were capped.

Estimate turbulent dissipation rate at the water surface

EFDC includes the Mellor-Yamada turbulence closure model. Its output can be used to simulate the turbulence dissipation rate ε as below (Mellor and Yamada, 1982; and Burchard, 2001):

$$\varepsilon = \ q^3/(B_1\, l) \tag{2.2}$$

where *q* = the turbulent velocity scale (m/s); *l* = the macro length scale of turbulence (m); and B_1 = an empirical parameter in the turbulence model = 16.6.

The Mellor−Yamada turbulence model in EFDC calculates *q* and *l* at the vertical layer interfaces in the water column (Tetra Tech, 2007), and the results closest to the air-water interface are located at the bottom of surface layers. For proper representation of DO transfer across the air-water interface, an extrapolation procedure similar to that presented in Section 1 was used for estimating ε at the air-water interface. To avoid negative results, we employed loglinear

interpolation of the output of the model grid, rather than either the linear or polynomial curve-fitting options presented in Section 1 of this appendix, to extrapolate to the air-water interface.

A laterally constrained and localized-sigma coordinate (GVC) grid system was chosen in this study to represent the lateral bathymetry variation in the Delaware Estuary efficiently and accurately (DRBC, December 2021 Draft). This coordinate configuration resulted in the number of active vertical layers varying from 1 to 12. The turbulence model is not applied to the cells with only one active vertical layer in EFDC. Instead, the logarithmic Law of the Wall is applied for estimating the dissipation rate in this situation (Burchard et al., 1998; Inoue et al., 2011; and Brumer et al., 2016):

$$\varepsilon = (u_*^3)/\kappa z \tag{2.3}$$

where u_* = the friction velocity (m/s) = $\sqrt{\tau_b/\rho_w}$; τ_b= bed shear stress (N/m^2), ρ_w= water density (kg/m^3); κ = von Karman constant = 0.4; and z = height above the bed (m).

Note that the turbulent dissipation rate in the reaeration calculation (i.e., Equation 2.2) reflects the turbulence at the water surface, based on the turbulent velocity scale and macro scale at the surface segments. One exception is for the very upstream portion of the River delineated by nine segments, where there is only one vertical layer and the turbulence model in EFDC is not activated. The surface turbulent dissipation rates in these nine segments are approximated by the logarithmic Law of the Wall (i.e., Equation 2.3) and bed shear stresses.

3. COMPARISONS OF DISSOLVED OXYGEN RESULTS BETWEEN ZAPPA'S APPROACH AND CONVENTIONAL METHODS

By DRBC

WASP contains several conventional approaches for calculating reaeration, e.g., Covar (1976), O'Connor-Dobbins (1958), Owens et al. (1964), Churchill at al. (1962), and Tsivoglo-Wallance (1972). These were originally derived for river and stream environments and use water column depth and depth-averaged velocity for calculating the mass transfer coefficient. In this section, the O'Connor-Dobbins approach was selected for comparison with Zappa's approach.

The O'Connor-Dobbins approach includes hydraulic-driven and wind-driven mass transfer coefficients. In rivers and streams where reaeration is dominated by current velocity, the hydraulic-driven mass transfer coefficient at 20°C is given as (Chapra, 1997):

$$K_L = 3.93\sqrt{\frac{U}{H}} \tag{3.1}$$

where K_L = the liquid film mass transfer coefficient (m/d); U = depth-averaged velocity (m/s); and H = water column depth (m).

For open waters with large fetch, such as bays and wide estuaries, wind becomes the predominant factor in causing reaeration. O'Connor (1983) developed a set of equations for mass transfer coefficients of gases due to wind for both smooth and rough surface conditions.

Three WASP simulations were conducted for comparison, only varying the reaeration approach. These reaeration approaches were 1) Zappa's approach; 2) the O'Connor-Dobbins approach, summing the hydraulic- and wind-driven mass transfer coefficients, hereafter called O'Connor-Dobbins (Sum); and 3) O'Connor-Dobbins approach, choosing the maximum of the hydraulic- and wind-driven mass transfer coefficients, hereafter called O'Connor-Dobbins (Max).

Figure 3-1 presents the predicted and measured (near-) surface, daily averaged DO concentrations at four USGS stations and two buoy stations from Philadelphia Water Department (PWD) during 2018 and 2019. The top panels show DO time series comparisons and the bottom panels show comparisons of cumulative frequency distributions. DO sensors at USGS stations (i.e., Pennypack Woods, Ben Franklin Bridge, Chester, and Reedy Island) were installed 2–3 ft below the water surface during low tide, approximately corresponding to the second-from-the-surface vertical layer in the model. DO sensors at PWD buoy stations (i.e., Buoys B and P) were at about 1 m below water surface, corresponding to the model's surface layer.

All three approaches predicted similar seasonal variations (top panels in Figure 3-1) and similar ranges of higher end DO concentrations (bottom panels in Figure 3-1). However, lower end DO concentrations (i.e., 1st percentile and lower) are more critical from a regulatory perspective. DO concentrations in the Delaware Estuary typically reach minimum values during July-August, as the result of elevated nitrification, CBODU oxidation, and sediment oxygen demand caused by high water temperature. The ultimate impacts of three reaeration approaches on lower end DO concentrations are demonstrated in the bottom Panels of Figure 3-1. Zappa's approach matched well with observed lower end DO concentrations at three stations: Pennypack Woods, Ben

Franklin Bridge, and Buoy P; and over-predicted lower end DO concentrations by about 0.2–0.4 mg/L at the other stations: Buoy B, Chester, and Reedy Island. The O'Connor-Dobbins (Sum) approach consistently over-predicted DO concentrations at the lower end by about 1.0 mg/L more than the Zappa approach. The O'Connor-Dobbins (Max) approach predicted almost identical results to the Zappa approach in the upper portion of the river (i.e., Pennypack Woods and Ben Franklin Bridge). In contrast, moving downstream (i.e., Buoy B, Chester, Buoy P, and Reedy Island), the O'Connor-Dobbins (Max) approach over-predicted the lower end DO concentrations by about 0.2–0.4 mg/L more than the Zappa approach.

Figure 3-2 illustrates vertical profiles of predicted and measured DO concentrations across four transects near USGS stations during four different surveys: Pennypack Woods (RM 110.5) on July 24, 2019; Ben Franklin Bridge (RM 100) on December 4, 2019; Delaware Memorial Bridge (RM 68.9) on July 19, 2018; and Reedy Island (RM 54) on June 7, 2019. The observed DO concentrations for different vertical profiles are shown as dots and grouped into model grid cells, with different colors (e.g., red, orange, and magenta) representing the separate measurement profiles that occurred within a single EFDC model grid location. The values of Mod I represent the model cell IDs across the transects from Pennsylvania shore (the smaller values) to New Jersey shore (the larger ones). These vertical profile data reflect the common perception that the Delaware Estuary is relatively well mixed or weakly stratified, e.g., about 0.5 mg/L differences in DO concentration from the surface to bottom. Lateral variation showed similar differences in DO concentrations, with New Jersey shore being higher generally than the Pennsylvania shore. Model results are shown as lines in Figure 3-2. All three simulations reproduced similar vertical and lateral structures as the measured ones, although uncertainties exist in terms of the exact timing and location between the predicted and measured values. Among the three approaches, Zappa's achieved the best model–data comparison, i.e., almost on top of measured profiles at the two upstream transects near Pennypack Woods and Ben Franklin Bridge (except at one shallow cell near New Jersey shore), and over-prediction of DO concentrations up to about 0.5–0.8 mg/L at the two downstream transects near Delaware Memorial Bridge and Reedy Island. The O'Connor-Dobbins (Sum) approach consistently over-predicted the DO profiles by 0.5 mg/L or more than the Zappa approach. The O'Connor-Dobbins (Max) approach predicted almost identical profiles to the Zappa approach at the two upstream transects and over-predicted the DO profiles by about 0.2 mg/L more than the Zappa approach at the two downstream transects.

The better performance of Zappa's method is likely attributed to the fact that this approach is more mechanistic in that: a) it utilizes the near-surface parameters (e.g., turbulence dissipation rate in the near-surface boundary layer), instead of the water column depth and depth-averaged velocity, to quantify the gas transfer at the air–water interface; and b) it incorporates the comprehensive effects of current velocity, wind speed, and water temperature on reaeration into the key parameters ε and Sc. As a result, model users do not need to decide whether to use hydraulic- or wind-driven formulations. In nature, these comprehensive effects may not function in a linear superposition manner, suggesting why the approach of O'Connor-Dobbins (Sum) tended to over-predict the DO concentrations. In the upper portion of the river where fetch is small and current velocity dominates the reaeration, Zappa's approach predicted almost identical DO concentrations to the commonly used hydraulic-driven formulation from O'Connor-Dobbins. This further supports the validity of Zappa's approach. In the downstream portion of the river where both current velocity and wind play important roles in reaeration, Zappa's approach incorporates the comprehensive effects of current and wind on reaeration in a more mechanistic, hence better manner, than the approach of O'Connor-Dobbins (Max).

More comparisons and applications may be needed to further validate Zappa's approach for simulating reaeration for other sites and types of waterbodies. Nevertheless, adding this approach to the WASP options of reaeration simulation certainly enhances the WASP model's capability for simulating the effects of reaeration on water column DO in the Delaware Estuary.

Figure 3-1a: Model−Data Comparisons of Daily DO during 2018−2019 at USGS station Pennypack Woods

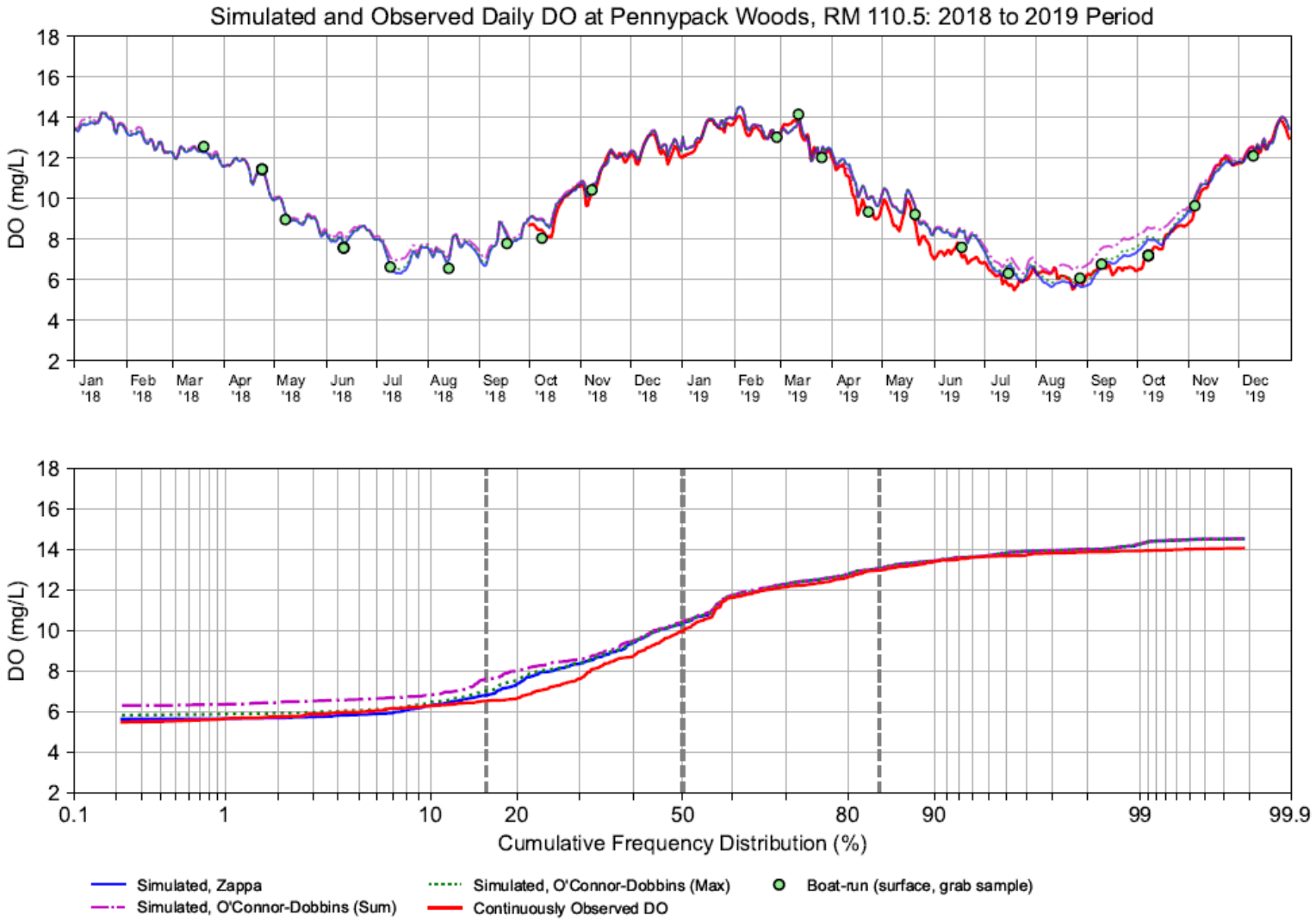

Figure 3-1b: Model−Data Comparisons of Daily DO during 2018−2019 at USGS Station Ben Franklin Bridge

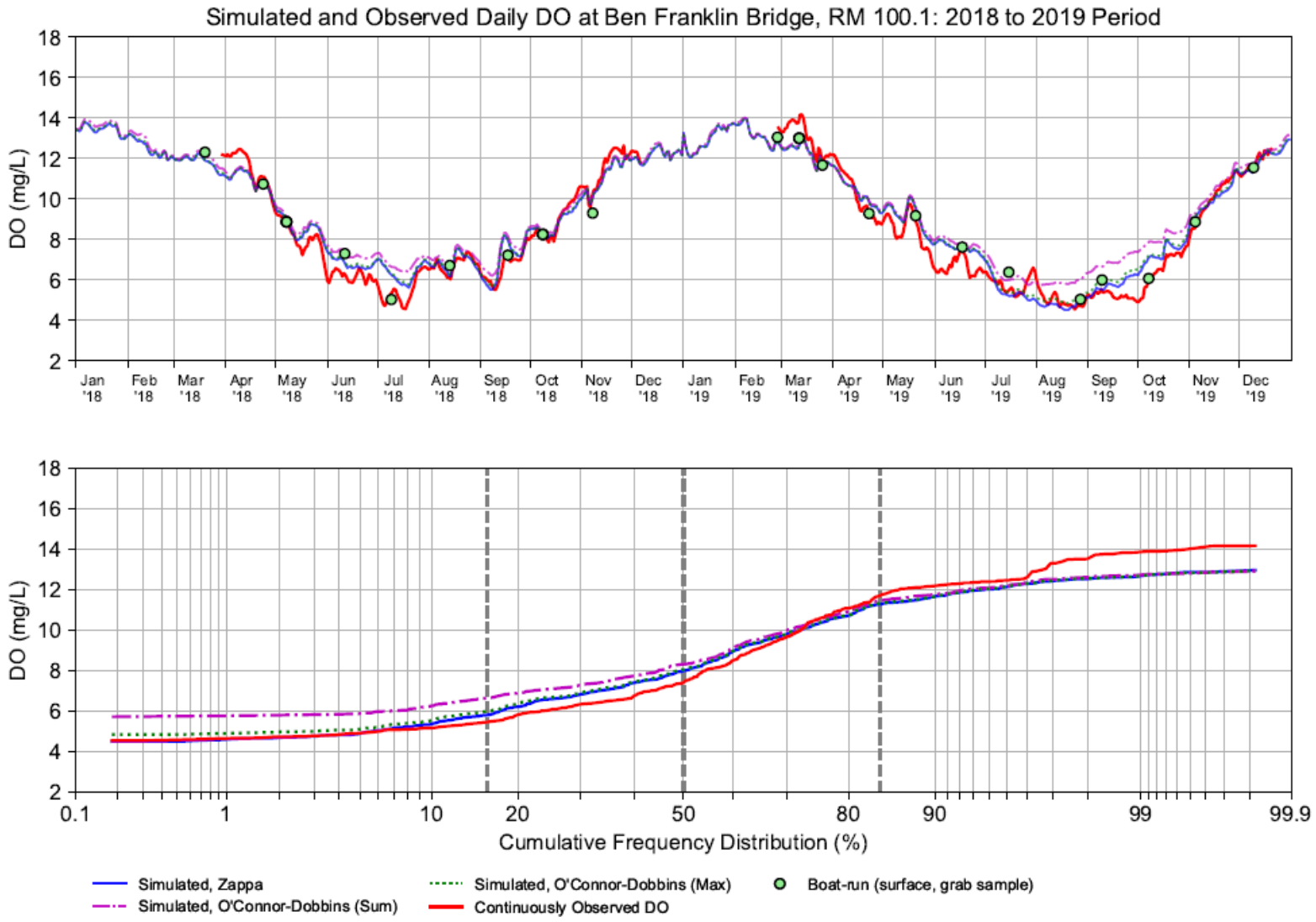

Figure 3-1c: Model−Data Comparisons of Daily DO during 2018−2019 at PWD Buoy B

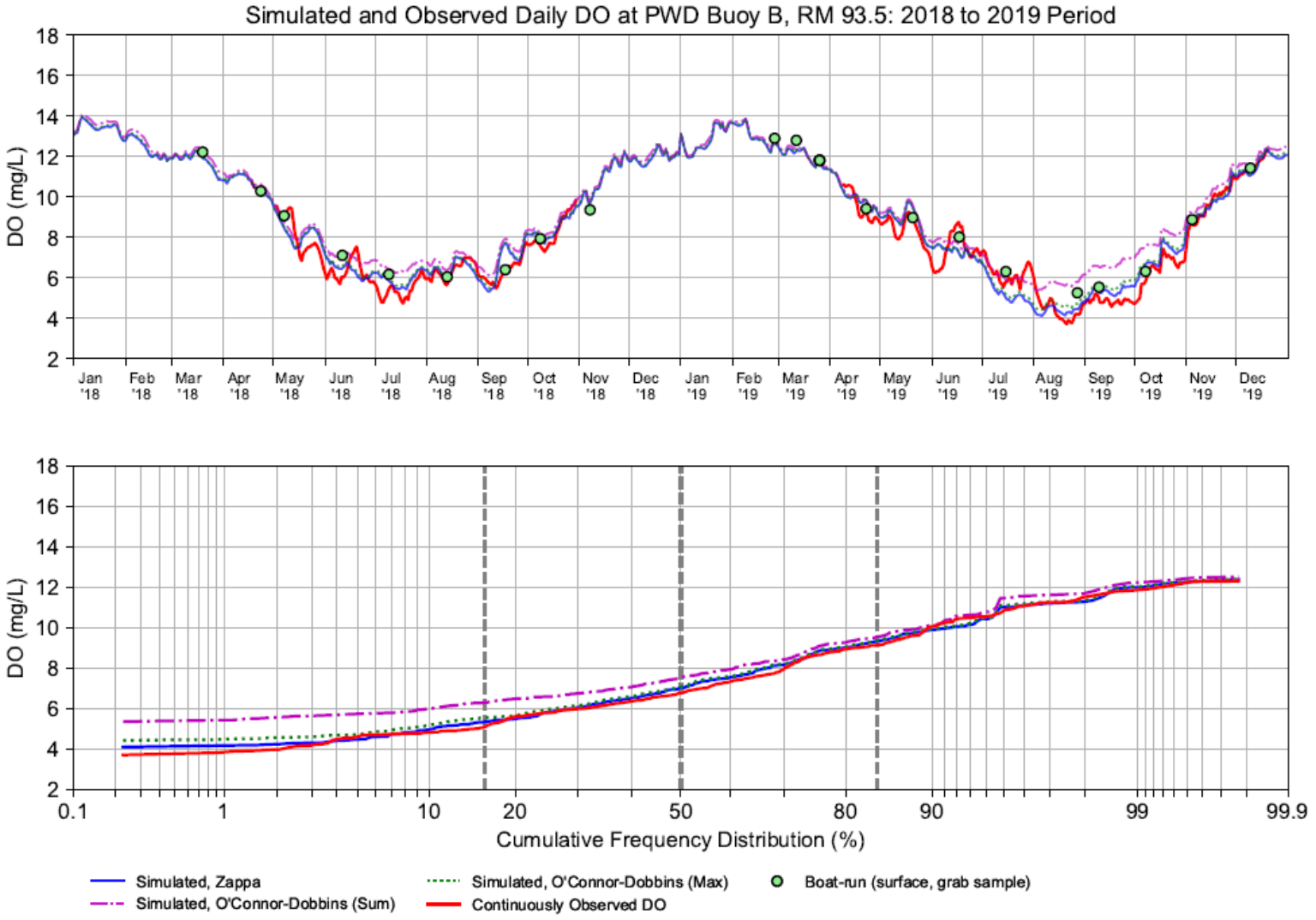

Figure 3-1d: Model−Data Comparisons of Daily DO during 2018−2019 at USGS Station Chester

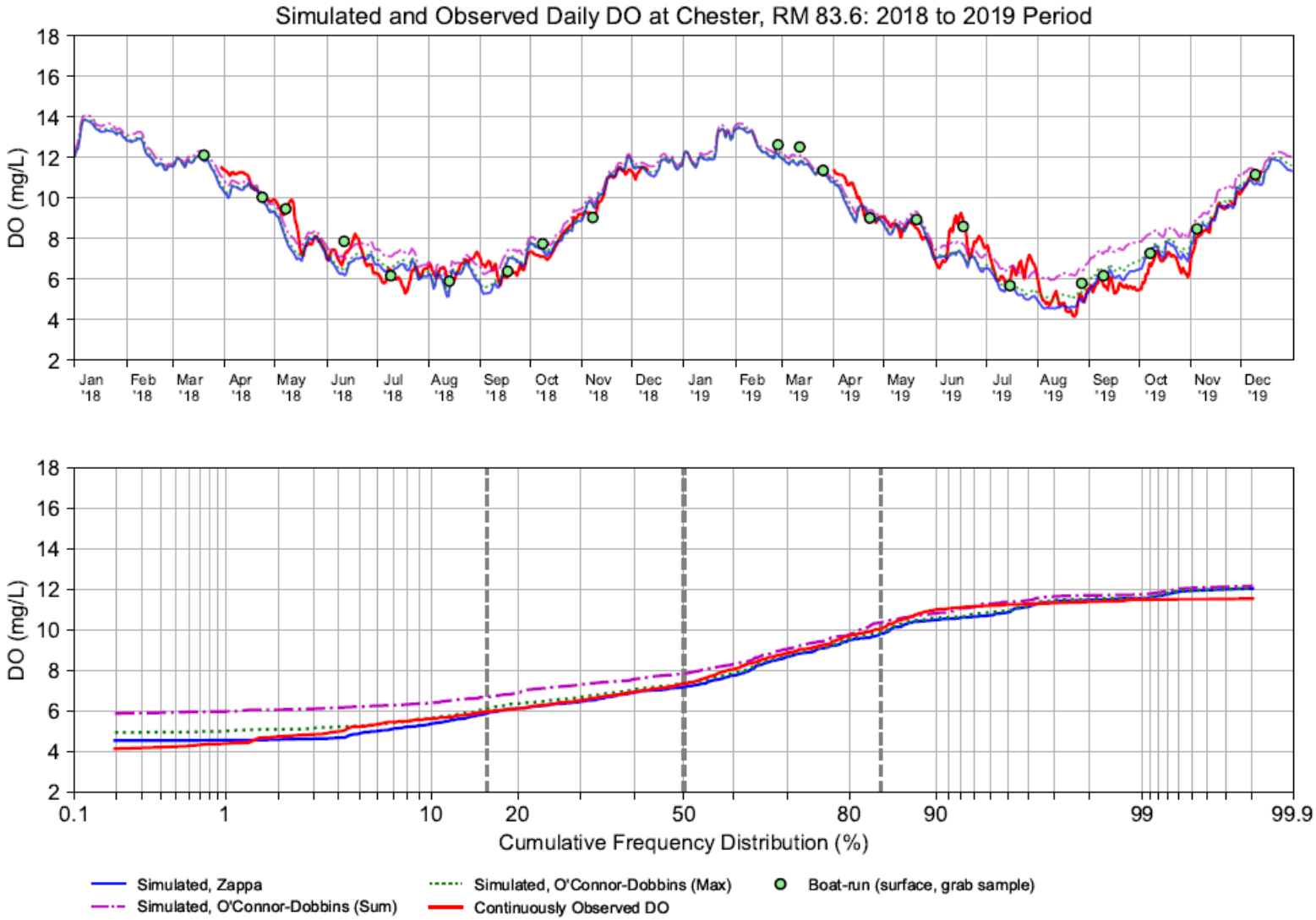

Figure 3-1e: Model−Data Comparisons of Daily DO during 2018−2019 at PWD Buoy P

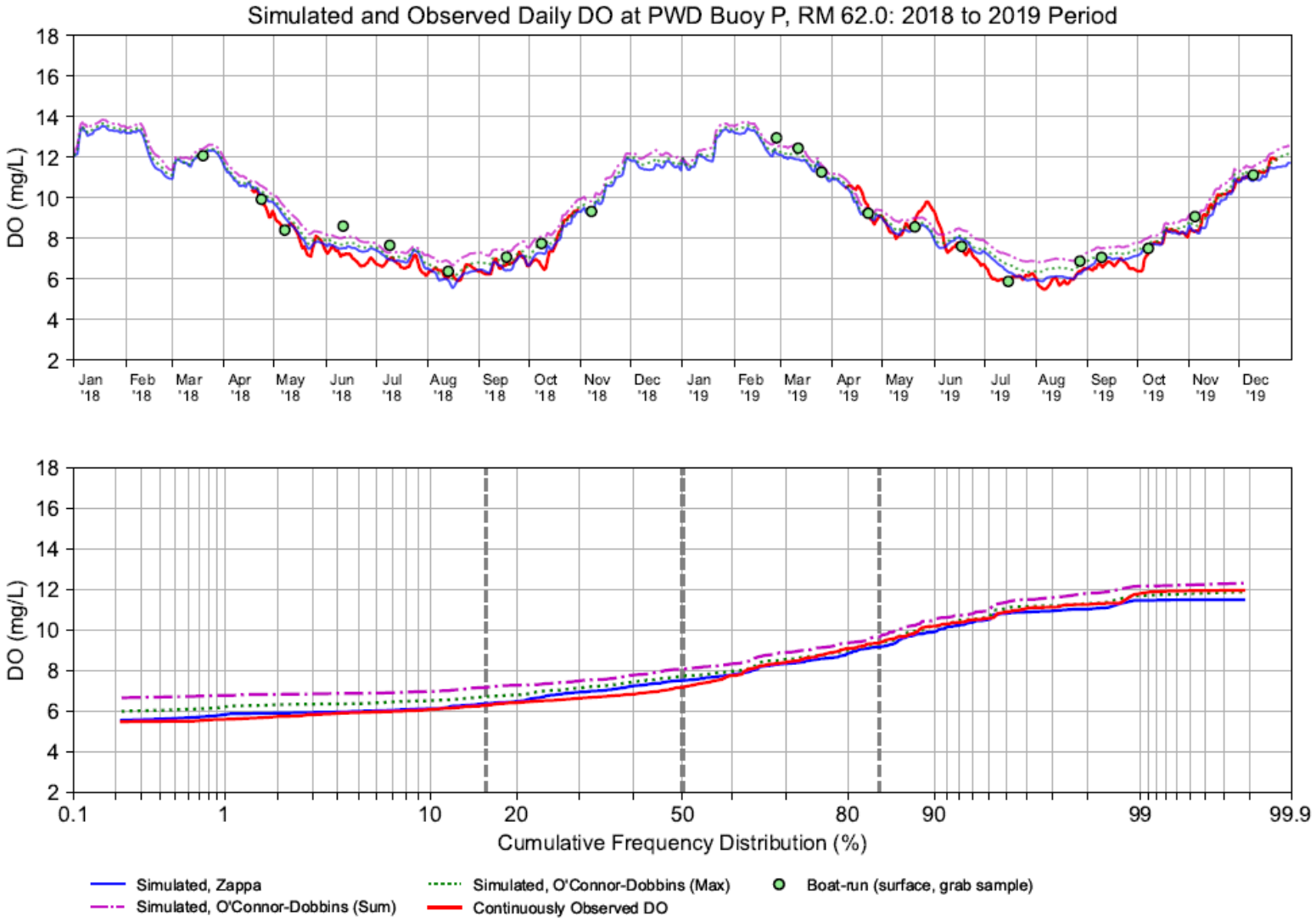

Figure 3-1f: Model−Data Comparisons of Daily DO during 2018−2019 at USGS Station Reedy Island

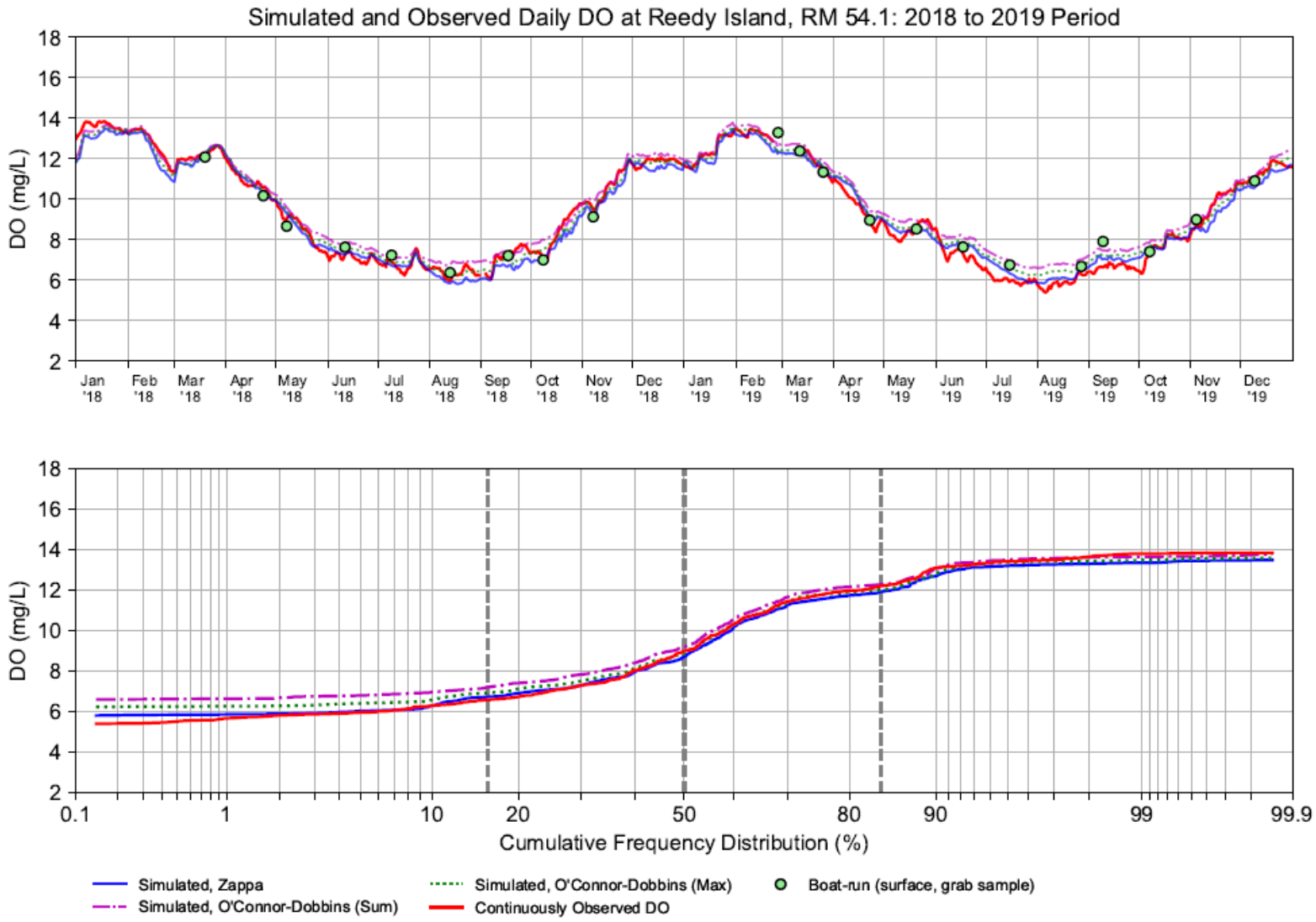

Figure 3-2a: Model to Transect Data Comparisons

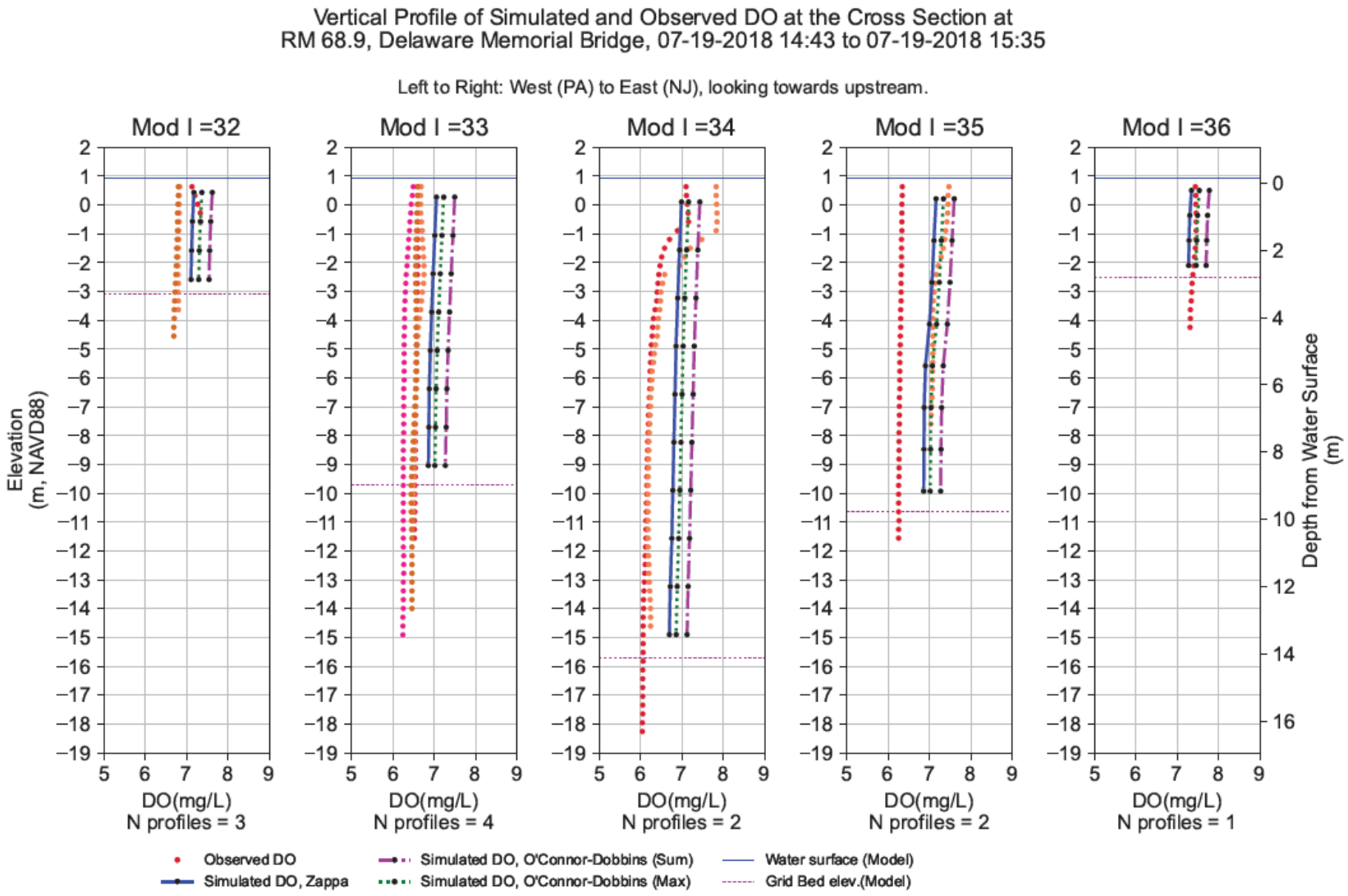

Figure 3-2b: Model to Transect Data Comparisons

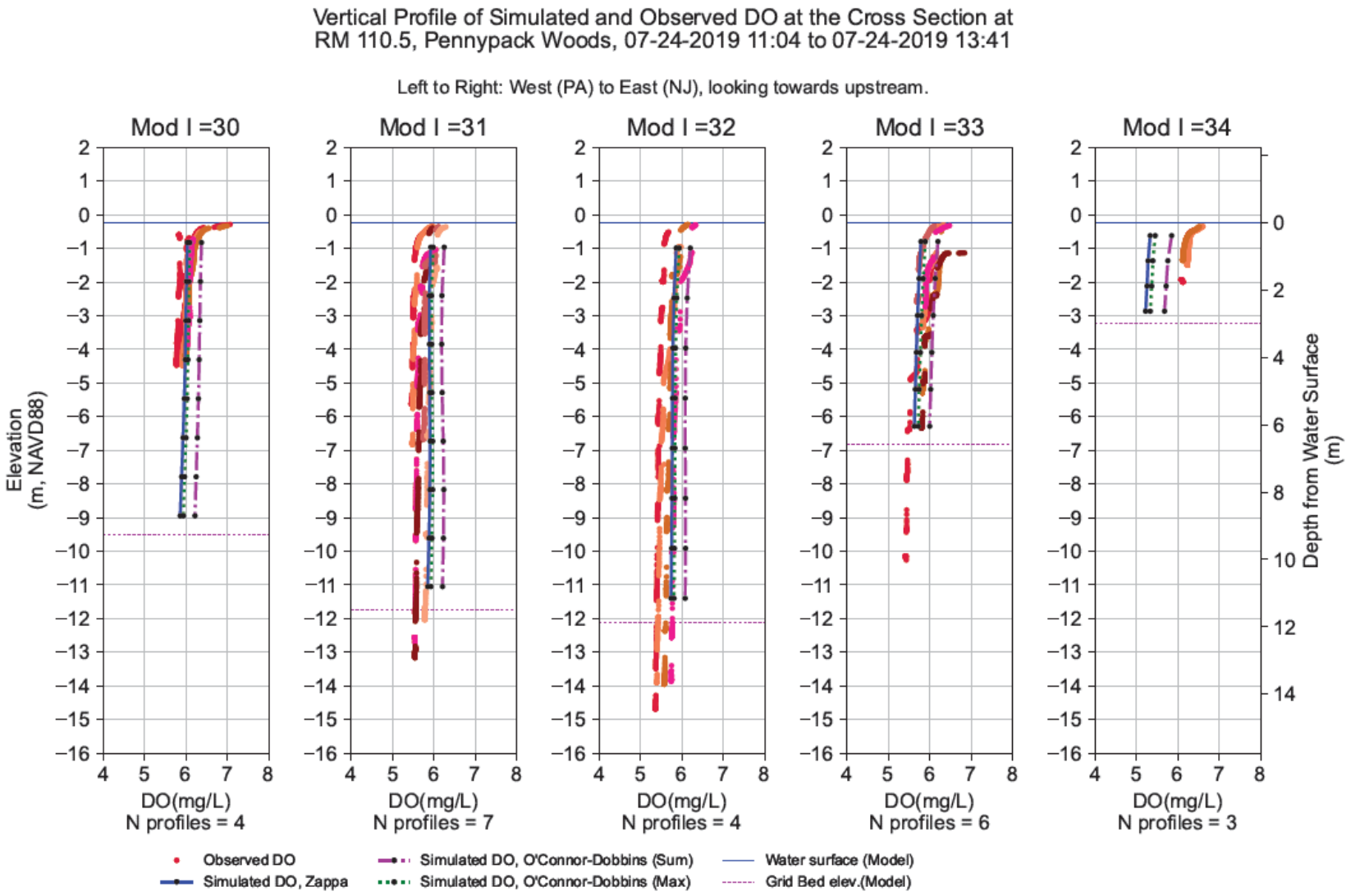

Figure 3-2c: Model to Transect Data Comparisons

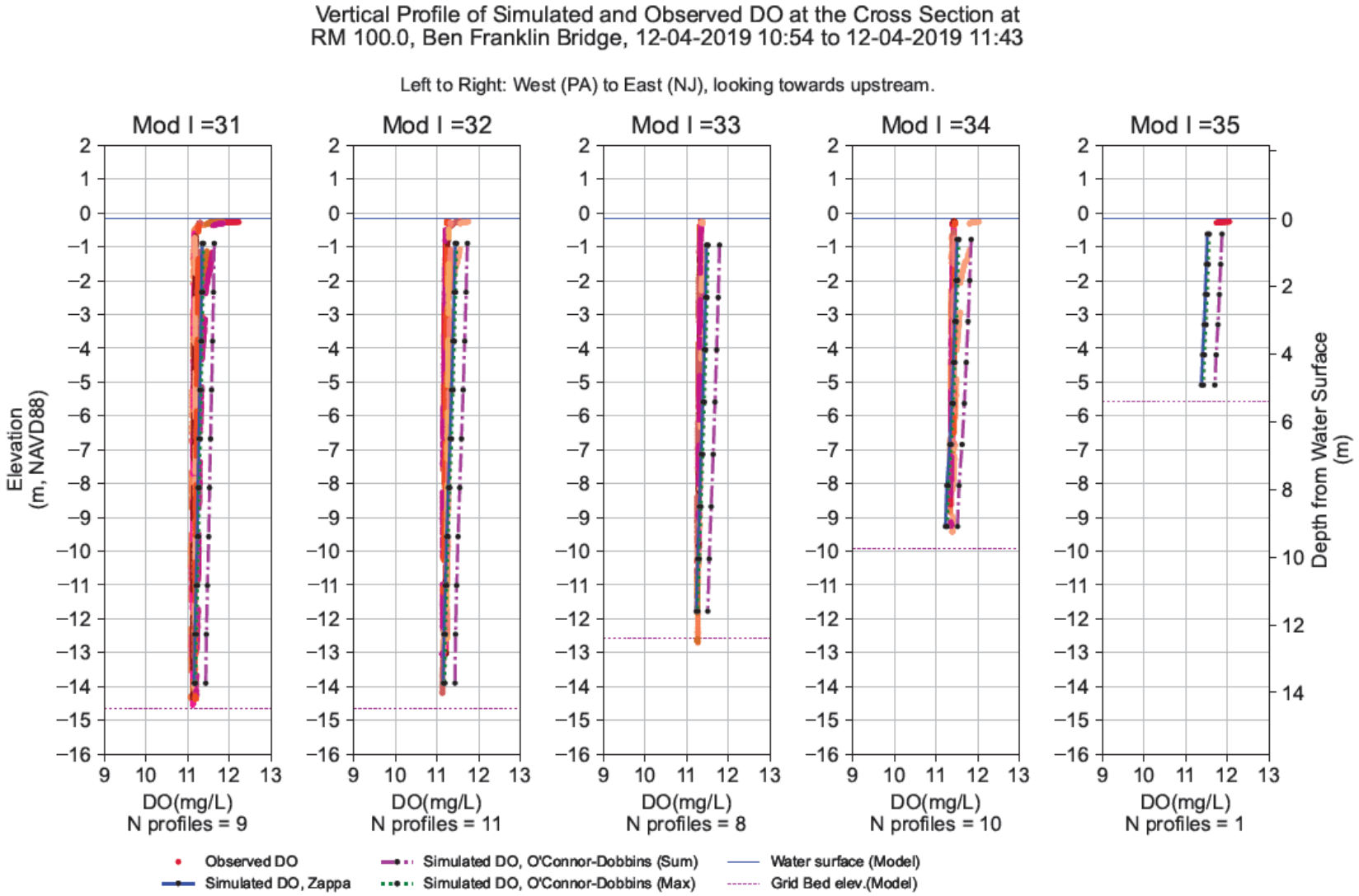

Figure 3-2d: Model to Transect Data Comparisons